Numerical analysis of flow mark surface defects in injection molding flow

Numerical analysis of flow mark surface defects in injection molding flow

Anne M. Grillet,[a] Arjen C. B. Bogaerds, and Gerrit W. M. Peters, and

Frank P. T. Baaijens[b]

Dutch Polymer Institute, Department of Mechanical Engineering, Eindhoven University of Technology, Postbus 513, 5600 MB Eindhoven, The Netherlands

Markus Bulters

DSM Research, P.O. Box 18, 6160 MD Geleen, The Netherlands

(Received 30 May 2001; final revision received 7 January 2002)

Synopsis

In order to elucidate the mechanism of flow mark surface defects, the stability of injection molding flow is investigated numerically using a transient finite element method. Experiments performed by Schepens and Bulters [Bulters, M., and A. Schepens, ''The origin of the surface defect 'slip-stick' on injection moulded products,'' Paper IL-3-2, in *Proceedings of the 16th Annual Meeting of the Polymer Processing Society*, Shenghai, China, 2000a, pp. 144–145] using a novel two color injection molding technique are summarized and they indicate that surface defects are caused by a flow instability near the free surface during filling of the mold. Steady finite element calculations of a model injection molding flow using a single mode, exponential Phan-Thien–Tanner constitutive equation supply information about the base state streamlines and polymer stresses. By varying the parameters of the model, the degree of strain hardening in the extensional viscosity can be controlled. Then a linear stability analysis is used to determine the most unstable eigenmode of the flow and the dependence on the extensional properties of the polymer. For strain softening materials, the injection molding flow is predicted to be stable up to a Weissenberg number of five. However, the most unstable disturbance is consistent with the swirling flow near the interface observed experimentally. For strain hardening rheologies, an instability is observed in the channel flow far from the interface, in agreement with calculations performed by Grillet *et al.* [Grillet, A. M., A. C. B. Bogaerds, G. W. M. Peters, and F. P. T. Baaijens, ''Stability analysis of constitutive equations for polymer melts in viscometric flows,'' J. Non-Newt. Fluid Mech. (accepted, 2001)] on planar Poiseuille flow of a Phan-Thien–Tanner fluid. © *2002 The Society of Rheology.* [DOI: 10.1122/1.1459419]

I. INTRODUCTION

Flow instabilities during injection molding can cause nonuniform surface reflectivity on a plastic product. Our research focuses on a specific surface defect that is characterized by shiny dull bands roughly perpendicular to the flow direction which alternate on the upper and lower surfaces of the mold as shown in Fig. 1. These defects, which are

[a]Current address: Sandia National Laboratories, P.O. Box 5800, MS 0834, Albuquerque, NM 87185.
[b]Author to whom all correspondence should be addressed; Electronic mail: baaijens@wfw.wtb.tue.nl

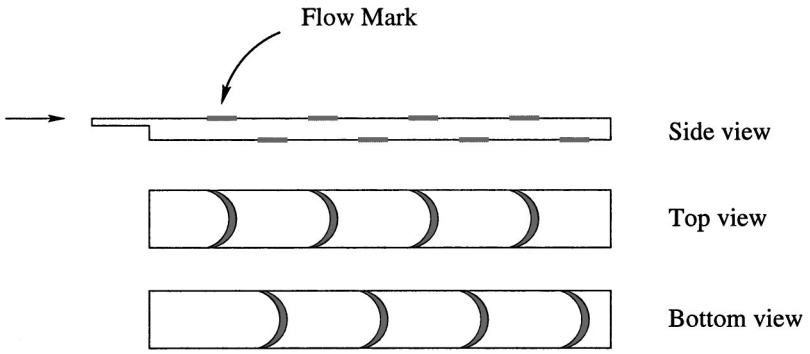

FIG. 1. Characteristic pattern for flow mark surface defects.

referred to as flow marks, tiger stripes, or ice lines, have been observed in a variety of polymer systems including polypropylene [Bulters and Schepens (2000a)], acrylonitrile-styrene-acrylate (ASA) [Chang (1994)], ethylene-propylene block copolymers [Monasse *et al.* (1999)] and polycarbonate (PC)/acrylonitrile butadiene-styrene (ABS) blends [Hobbs (1996); Hamada and Tsunasawa (1996)]. The occurrence of these defects can limit the use of injection molded parts, especially in unpainted applications such as car bumpers.

The nature of the alternating bands depends on the polymer material. With polypropylene and ASA injection molding, flow marks appear as dull, rough bands on a normally smooth, shiny surface [Bulters and Schepens (2000a); Chang (1994)]. Scanning electron micrographs show that the region with flow marks has a striated surface topology that shows hills and valleys oriented in the flow direction [Chang (1994)]. For polymer blend systems, Hamada and Tsunasawa (1996) suggested that the differences in reflectivity can also be associated with differences in the blend composition at the flow marks. During steady injection molding of PC/ABS blends, the authors noted that the polycarbonate phase seems to preferentially coat the mold wall, leaving a shiny surface [Hamada and Tsunasawa (1996)]. By contrast, the flow mark bands were found to contain a higher concentration of ABS and were cloudy. By selectively etching the ABS component, approximate streamline patterns could be observed on cross sections of the injection molded product [Hamada and Tsunasawa (1996)]. When the smooth, PC rich surface was being deposited, the blend morphology showed a symmetrically smooth flow pattern near the free surface. However, when the flow front passed through the region where flow marks were being deposited on the mold surface, the steady flow pattern near the free surface had been disrupted and was no longer symmetric [Hamada and Tsunasawa (1996)].

Other recent experimental findings have also concluded that the surface defects are the result of an unstable flow near the free surface similar to that shown in Fig. 2 [Bulters and

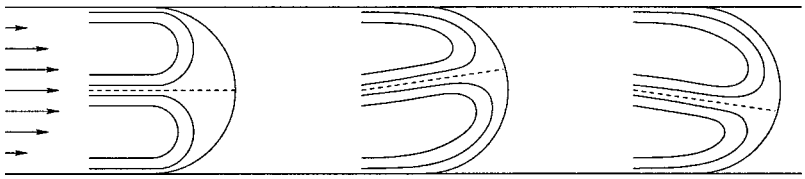

FIG. 2. Unstable flow may cause surface defects.

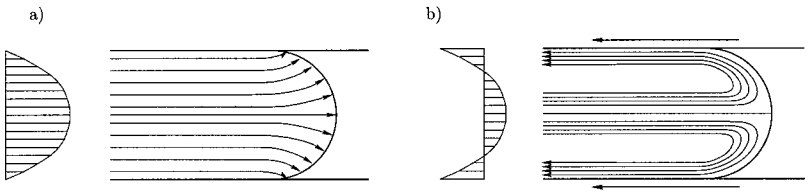

FIG. 3. Kinematics of the fountain flow region: reference frame of (a) the mold and (b) the moving interface.

Schepens (2000a); Chang (1994); Hobbs (1996); Hamada and Tsunasawa (1996); Monasse *et al.* (1999)]. The two most common mechanisms that have been proposed for unstable flow are slip at the wall [Chang (1994); Hobbs (1996); Monasse *et al.* (1999)] or instability at the point of stagnation [Bulters and Schepens (2000a); Monasse *et al.* (1999)]. Due to the limited availability of rheological data, there is no clear understanding of the rheological dependence of the instability, although Chang (1994) found that materials with a higher recoverable shear strain ($S_R = N_1/2\tau_{xy}$) had less severe flow mark surface defects.

A similar unstable flow was postulated to explain the transfer of pigments during injection molding of high density polyethylene [Reilly and Price (1961)]. If a small amount of red pigment or crayon were placed on one mold surface, a transfer mark would be present on the *opposite* wall downstream of the original mark. The transfer was attributed to an ''end-over-end'' flow pattern which was found to depend on the injection speed and mold thickness. The type of polymer was also important because transfer marks were not observed for a cellulose acetate or a polystyrene polymer [Reilly and Price (1961)]. Wall slipping has been proposed as a possible mechanism for the transfer marks [Denn (2001)], but they may also have been caused by the same flow instability that causes flow mark surface defects [Wissbrun (2001)].

Because of the complexity of the industrial injection molding process (three-dimensional, nonisothermal flow; fully elastic material rheology with many time scales; crystallization; fiber or particulate reinforcement) it is not possible to address every aspect fully [Isayev (1987)]. There has been a large amount of work that has focused on different components of the complete injection molding process. For example, the kinematics of injection molding of inelastic shear thinning materials are fairly well understood [Isayev (1987)]. Whereas no simulations have been performed to specifically investigate flow mark surface defects, the fountain flow near the advancing free surface (where stagnation point instability has been postulated) has been investigated, initially by Rose in 1961. As fluid elements move towards the advancing interface, they ''spill over towards the wall region being vacated by the advancing interface'' [Rose (1961)] as illustrated in Fig. 3(a).

The effect of fountain flow on quenched stresses in injection molded products was examined in detail by Tadmor (1974) and more recently by Mavridis *et al.* (1988). The deformation history of the fluid elements in the fountain flow can have a significant impact on the molecular orientation and trapped stresses in an injection molded product. This is especially true in the surface layer since material which is deposited on the mold's surface with the polymers in a stretched state will rapidly be cooled and create a ''skin layer'' with high residual stress. Material in the core region cools more slowly so the polymer stretch and orientation can relax [Mavridis *et al.* (1988); Tadmor (1974)]. Since it is the skin layer which determines surface reflectivity, the uniformity of the elongational flow at the point of stagnation will have a direct impact on surface quality.

There can be significant difficulties in incorporating elasticity into simulations of free surface flow because of the geometric ''stick–slip'' singularity that exists at the point of contact where the free surface intersects the mold wall, as summarized by Shen (1992). Elastic constitutive equations are known to make geometric singularities more severe [Grillet *et al.* (1999); Hinch (1993)]. In order to make elastic injection molding simulations tractable, many researchers have incorporated slip along the wall near the singularity [Sato and Richardson (1995); Mavridis *et al.* (1988)]. Various formulations for a slip condition do not seem to have a strong effect on the kinematics in the free surface, but all seem to ease the difficulties associated with numerical calculations, especially for elastic constitutive equations [Mavridis *et al.* (1986); Mavridis *et al.* (1988); Shen (1992)].

Perhaps due to the difficulties associated with the geometric singularity, there have been few fully elastic simulations of injection molding flow (i.e., coupled velocity and stress calculations with an elastic constitutive equation) [Kamal *et al.* (1988)]. Most simulations have instead assumed Newtonian flow or otherwise used constitutive models which incorporated shear thinning, but not elastic effects such as the power law model [Tadmor (1974); Mavridis *et al.* (1986)]. The few studies which have used more realistic constitutive equations such as the Leonov model [Mavridis *et al.* (1988)]; the White–Metzner model [Kamal *et al.* (1986) (1988)], and the Oldroyd-B model [Sato and Richardson (1995)] mostly focused on modeling the deformation of tracer particles by the fountain flow or predicting quenched elastic stresses in the final product; they unfortunately did not investigate the stresses in fountain flow. As for other complex flows such as flow around a cylinder, there have been numerous studies using various numerical methods and viscoelastic constitutive equations and they are summarized in a recent review by Baaijens (1998).

We have performed steady, transient finite element simulations of a viscoelastic fluid in a simplified injection molding flow to investigate the occurrence of flow mark surface defects. A fully implicit DEVSS-G/SUPG method which was thoroughly tested on planar flows of viscoelastic materials [Grillet *et al.* (in press)] is applied to the model flow. The exponential version of the Phan-Thien–Tanner constitutive equation was chosen because it can qualitatively capture the rheology of polymer melts [Larson (1988)]. By varying the parameters of the model, melts ranging from strain hardening to strain softening in extensional flow can be investigated for their effect on fountain flow. Before discussing details of the simulations, we review some recent experiments on flow mark surface defects which were instrumental in the design of the simulations [Bulters and Schepens (2000a, 2000b)].

II. EXPERIMENTAL RESULTS

A series of injection molding experiments were carried out on several commercial, impact modified polypropylene compounds (DSM). The tests were performed on a standard bar shaped ruler mold with a length of 300 mm long, 30 mm wide, and 3 mm thick. The frequency and severity of the flow mark surface defects were recorded as a function of several molding parameters including the mold and melt temperatures and the mold design as well as geometric factors such as the mold width, the injection screw diameter, and the buffer size. From the results, several potential mechanisms which had been proposed to explain the occurrence of flow marks were discarded. Because the defects did not depend on the buffer size or screw and nozzle geometry, the possibility of upstream instability in the nozzle or gate was ruled out. The mold surface was modified by coating the mold with a very thin layer of silicone oil or coating one side of the mold with fluoropolymer, but this had no effect on the frequency of the surface defect so slip at the

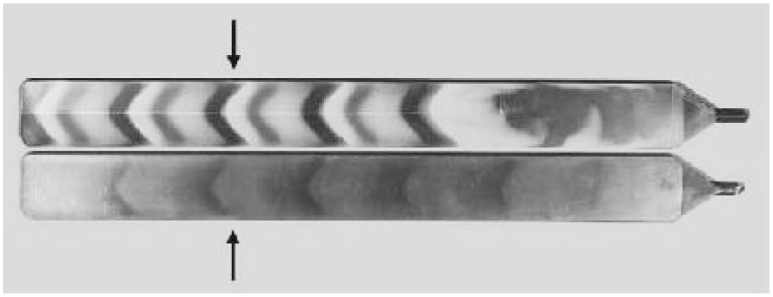

FIG. 4. Two color injection molding experiment (above) compared with a traditional injection molded sample (below).

wall was discarded as the cause of the flow marks. That left the possibility of an instability during filling of the mold.

To further investigate this as a possible mechanism, a new two color injection molding technique was developed. The ruler mold was filled with a polymer whose bottom 47% had been dyed black. If the flow is stable, white material should flow along the symmetry line in the center towards the free surface where it will be split by the point of stagnation, leaving a thin coating on the top and bottom surfaces of the bar. Instead, the surface of the bar displayed alternating black and white strips which corresponded both in location and frequency to the surface defects in the original experiments (Fig. 4). This technique allows investigation of the causes of surface defects, independent of the crystallization behavior, once the polymer begins to solidify on the cold mold wall.

Short-shot experiments were also performed using the two color injection molding technique. Fittings were placed in the mold that allowed the ruler mold to be filled only partially. These experiments were carried out using a block of white polymer with a thin strip of black polymer along its centerline. The results for a series of tests where the mold was filled to different volume fractions is shown in Fig. 5. In a stable flow, the black material should coat both mold surfaces. However, instead of the symmetric fountain flow pattern expected at the interface, the black strip is first swept to the bottom then flipped around to the top. The alternating colors of the surface coating match exactly the black and white stripped pattern observed when the mold is completely filled. The oscil-

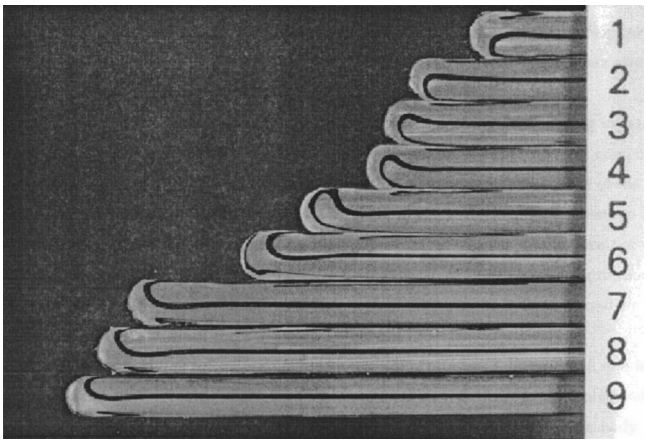

FIG. 5. Short shots with two color injection molding of a filled polypropylene compound.

latory flow pattern has also been confirmed using a high speed video of the mold filling process using a thin colored stripe injected along the centerline of a clear matrix. These results clearly strengthen the argument that surface defects are caused by instability in the fountain flow. The effects of the flow instability are only apparent in the fountain flow region and in the thin skin layer on the surface of the finished product. The channel flow far from the free surface remains free of instability.

Using these two color injection molding experiments, the dependence of the instability on various parameters was reexamined. One surprising result is that the instability does not depend on the mold temperature. However, the visibility of the surface defects in traditional injection molding experiments is strongly dependent on the mold temperature. For high enough mold temperatures, the surface defect disappears because the polymers are able to relax before they solidify, but the two color injection molding shows that flow instability is not affected.

These experimental results have led us to make several simplifying assumptions when designing the model injection molding problem for our numerical simulations. We will focus on two-dimensional injection molding flow. Since the instability does not depend on the temperature of the mold wall, isothermal calculations will be performed, neglecting temperature effects. Also, the interface is assumed to be a nondeformable semicircle. These are assumptions which we make so that transient simulations for an elastic constitutive equations are tractable with the computer resources which are available.

III. FINITE ELEMENT SIMULATIONS

For inertialess, incompressible flows, the dimensionless equations of the conservation of mass and momentum can be written as

$$\nabla \cdot u = 0, \tag{1}$$

$$\nabla \cdot \Pi = 0, \tag{2}$$

where u is the velocity vector. The components of the Cauchy stress tensor Π can be separated as $\Pi = -pI + \tau$ in terms of the pressure p and the polymer stress τ.

To complete the governing equations, a constitutive equation which relates the polymer stress to the rate of deformation must be defined. The dimensionless upper convected form of the exponential Phan-Thien–Tanner constitutive equation for a polymer melt is

$$Wi \overset{\nabla}{\tau} + \exp[\varepsilon Wi \, \mathrm{tr}(\tau)]\tau = \mathcal{D}, \tag{3}$$

where ε is a parameter, and $\mathcal{D} = \nabla u + (\nabla u)^T$ is the rate of strain tensor. The upper convected derivative is defined as

$$\overset{\nabla}{\tau} = \frac{\partial \tau}{\partial t} + u \cdot \nabla \tau - \tau \cdot \nabla u - (\nabla u)^T \cdot \tau. \tag{4}$$

The Weissenberg number is based on the average shear rate across the channel far from the free surface as

$$Wi = \frac{U\lambda}{H} \tag{5}$$

in terms of the mean velocity U and the half channel height H. These equations have been nondimensionalized by H, U, and the zero shear viscosity. We focus on the upper convected form of the Phan-Thien–Tanner model because the use of the full form that incorporates the Gordon–Schowalter derivative causes a maximum in the shear stress as a function of the shear rate for some parameter values. Such a maximum has never been

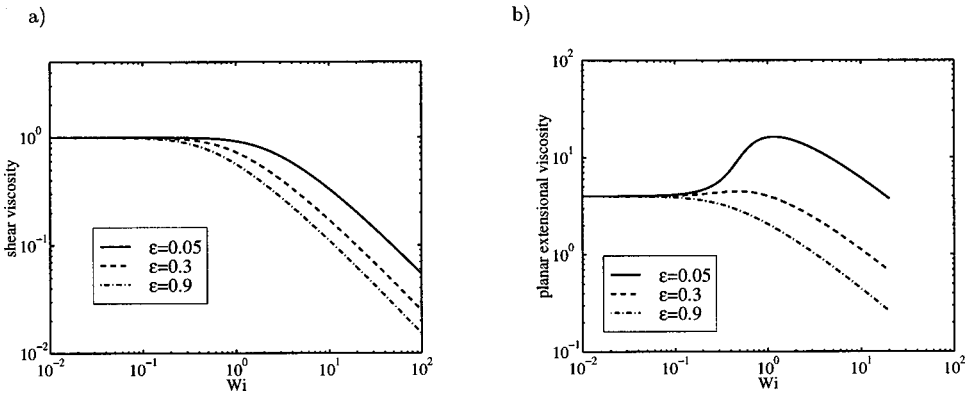

FIG. 6. Rheology of several model Phan-Thien–Tanner fluids with different values of ε: (a) steady shear and (b) planar extension.

observed experimentally and results in a discontinuous velocity profile in Poiseuille flow [Alves *et al.* (2001); Larson (1988); Saramito (1995)]. We examine several values of the adjustable parameter ($\varepsilon = 0.05,0.3,0.9$) which controls the degree of strain hardening in extension and also the onset of shear thinning of the shear properties as shown in Fig. 6. The linear viscoelastic parameters were held fixed for the three rheologies. Although multiple modes are usually required to capture the rheology of real (polydisperse) polymer melts [Larson (1988)], the present calculations to develop and test the numerical method use a single mode which admittedly can only qualitatively predict melt rheology. Multimode model calculations would be required to make quantitative comparison with experiments.

For our finite element calculations, the governing equations are written in a weak formulation using the stabilized, consistent DEVSS-G/SUPG method [Brooks and Hughes (1982)]. We have chosen this method because it has been shown to have excellent convergence properties in steady flow calculations in complex geometries [Baaijens (1998); Brooks and Hughes (1982); Grillet *et al.* (in press), Guénette and Fortin (1995); King *et al.* (1988); Talwar *et al.* (1994)].

$$\left(\phi_\tau + \frac{h}{|u|} u\cdot\phi_\tau, Wi\overset{\nabla}{\tau} + \exp[\varepsilon Wi\,\mathrm{tr}(\tau)]\tau - \mathcal{D}\right) = 0, \tag{6}$$

$$(\phi_v, \tau + \mathcal{D} - G - G^T) - (\nabla\cdot\phi_v, p) = 0, \tag{7}$$

$$(\phi_p, \nabla\cdot u) = 0, \tag{8}$$

$$(\phi_G, G - \nabla u) = 0, \tag{9}$$

with h the characteristic element size and (a, b) denotes the $\mathcal{L}_2$ inner product over the problem domain $\int_\Omega abd\Omega$. The polynomial spaces ϕ are chosen in the usual manner for low order finite elements to satisfy the Babuška–Brezzi (inf-sup) condition and for compatibility of the constitutive equation at stationary points: ϕ_v is biquadratic whereas ϕ_τ, ϕ_p, and ϕ_G are bilinear [King *et al.* (1988); Talwar *et al.* (1994)]. For steady base state flow calculations, the transient term in the upper convected derivative is ignored, and the equations are solved using a Newton iteration discussed earlier by others [Grillet *et al.* (1999, in press); King *et al.* (1988); Talwar *et al.* (1994)]. For the transient calculations, we treat the time derivative implicitly following Brown *et al.* (1993). Both steady and

FIG. 7. Typical finite element mesh containing 748 elements. The locations of the periodic boundary conditions are shown by the thicker vertical lines.

stability parts of this numerical method have been benchmarked on two planar flows previously [Grillet *et al.* (in press)].

To determine the stability of the flow once the steady solution $\tilde{\mathcal{X}} = (\tilde{u},\tilde{\tau},\tilde{p},\tilde{G})$ is attained, we employ a linear stability analysis. A small perturbation $\delta = (\hat{u},\hat{\tau},\hat{p},\hat{G})^T$ is added to the discretized governing equations [Eqs. (6)–(9)] and second order terms and higher are neglected. The resulting evolution equations for the perturbation variables are then solved as a function of time starting with a random initial perturbation to the polymer stresses. The transient calculations are continued until the $\mathcal{L}_2$ norm of the perturbation variables displays a constant growth or decay rate, or the magnitude of the perturbation has decreased below 10^{-5}. The constant growth or decay rate indicates that the transient calculation has isolated the most unstable eigenvalue or, more precisely, the eigenvalue with the largest (although not necessarily positive) real part of the eigenvalue.

A typical mesh (M41) used for the calculations is shown in Fig. 7. Constant velocity boundary conditions are imposed on the mold walls:

$$u(y = \pm 1) = -U. \tag{10}$$

For the moderate Weissenberg numbers used in this study (up to $Wi = 5$), local slip boundary conditions near the point of contact were not needed for this constitutive equation, perhaps because both the shear and extensional viscosities thin at high shear or strain rates. Other constitutive models such as the upper convected Maxwell model or the Giesekus model do exhibit difficulties with singularity in the form of a low limiting Weissenberg number ($W_i \approx 2$) beyond which calculations fail to converge and thus would require a local slip boundary condition. Also note that the mesh resolution in the neighborhood of the contact point is rather coarse since we have not attempted to resolve the singularity. Since the instability is believed to occur in the fountain flow upstream of the contact point, the behavior of the stability should not depend on the specific treatment of the contact point.

The free surface is a nondeformable, impenetrable, semicircular slip surface (i.e. normal velocity set to zero, but no boundary condition imposed on the tangential velocity). In simulations in the literature that have a deformable interface it was found that, even for shear thinning or elastic constitutive equations, the free surface shape stays nearly semicircular [Kamal *et al.* (1988)]. The stresses normal to the free surface are found to be small, although nonzero, except near the point of contact. Thus, we feel that the semicircular shape, while not perfect, is a reasonable assumption for our simplified model flow.

The inlet boundary conditions are handled in a unique way. Instead of specifying the known velocity profile for Poiseuille flow of a Phan-Thien–Tanner fluid, we instead impose periodic boundary conditions over the part of the channel marked by the thick lines in Fig. 7. To explain how this is implemented, we begin by writing the momentum equation for the nodes along the periodic boundary condition in an isolated channel.

TABLE I. Characteristics of the meshes used in the finite element computations.

Mesh	Length	Δy	No. of Elements
M3	9	0.2	172
M4l	12	0.1	748
M4ll	14	0.1	968
M4lt	22	0.1	1188
M6	9	0.0667	1608

$$(\phi_v, \tau + \mathcal{D} - G - G^T) - (\nabla \cdot \phi_v, p) + \int_{\Lambda_{\mathrm{PBC}}} \phi_v \Pi \cdot n \, d\Lambda = 0, \tag{11}$$

where $\Pi = -pI + \tau$ is the total stress, and n is the outward pointing normal vector of the element boundary. The boundary integral is performed over both sides of the channel's periodic boundary Λ_{PBC}. Because the velocities and stresses are identical across the periodic boundary, the boundary integral reduces to

$$\int_{\Lambda_{\mathrm{PBC}}} \phi_v \Pi \cdot n \, d\Lambda = (p_{\mathrm{outlet}} - p_{\mathrm{inlet}}) \int_{\Lambda_{\mathrm{PBC}}} \phi_v n \, d\Lambda. \tag{12}$$

When one side of the periodic boundary condition (PBC) is inside the geometry like in our model injection molding flow, we must include an additional boundary integral over the inlet to the fountain flow section (i.e., the sides of the elements along the right half of the internal periodic boundary). Then the momentum equation is

$$(\phi_v, \tau + \mathcal{D} - G - G^T) - (\nabla \cdot \phi_v, p) + \Delta p \int_{\Lambda_{\mathrm{PBC}}} \phi_v n d\Lambda + \int_{\Lambda_{\mathrm{internal}}} \phi_v \Pi \cdot n d\Lambda = 0. \tag{13}$$

This would be sufficient if the flow were driven by specifying the pressure drop Δp between the periodic boundaries. However, to specify the driving force as a total flux through the channel, the pressure drop Δp is replaced by a Lagrange multiplier l and an additional equation is added for the flux Q across the inlet.

$$(\phi_v, \tau + \mathcal{D} - G - G^T) - (\nabla \cdot \phi_v, p) + l \int_{\Lambda_{\mathrm{PBC}}} \phi_v \Pi \cdot n d\Lambda + \int_{\Lambda_{\mathrm{internal}}} \phi_v \Pi \cdot n d\Lambda = 0, \tag{14}$$

$$\int_{\mathrm{inlet}} u \cdot n d\Lambda = Q. \tag{15}$$

The Lagrange multiplier, and hence the pressure drop, is determined during the calculation. This formulation was chosen to simplify future comparison to injection molding experiments where generally the injection speed is known and also to simplify the stability calculations.

To validate our calculations, meshes of different lengths and levels of refinement were used (Table I). The coarsest mesh, M3, was not sufficient to resolve the steady flow of the shear thinning Phan-Thien–Tanner model at moderate Weissenberg numbers ($Wi > 2$). Since the stability calculations are the most demanding, data demonstrating convergence for the more refined meshes will be shown in Sec. III B. Unless otherwise

stated, the results presented here were taken from our medium refined mesh (M41) except for the lowest value of $\varepsilon = 0.05$ when a longer channel (M4lt with length = 22) was required for the stresses to fully develop between the fountain flow and the periodic boundary conditions at the highest Weissenberg numbers.

A. Steady results

We begin by presenting steady results for a range of ε parameters shown in Figs. 8–10 for $Wi = 3.0$. In Fig. 8 for the strain hardening material with $\varepsilon = 0.05$, we note the strong buildup of stress near the stagnation point on the free surface and also near the point of contact where the free surface intersects the moving wall. The relaxation of the stresses downstream of the interface enhances the flow near the free surface as shown by the compression of the streamlines towards the wall relative to the fully developed flow far from the free surface.

As ε is increased to 0.3, the onset of shear thinning is shifted towards lower Weissenberg numbers and the material also becomes more strain softening. These trends are reflected in both the stream function contours and the stresses. Due to the increased shear thinning, the velocity profile becomes more plug flow like in the pressure driven flow far from the interface and the velocity gradients are concentrated near the walls. Looking at the flow near the free surface, we note that the streamlines are shifted away from the interface and the strain rate near the stagnation point drops due to the strain softening extensional viscosity. This shift is also reflected in the polymer stress components. The maximum in the τ_{yy} stress has moved downstream of the stagnation point. As mentioned previously, the stresses downstream of the singularity decay more quickly for higher values of ε allowing the Poiseuille flow in the channel to reach equilibrium in fewer channel lengths. Hence the meshes used for this rheology are shorter than those required for the strain hardening material with $\varepsilon = 0.05$.

For the most strain softening rheology of $\varepsilon = 0.9$ shown in Fig. 10, the effects of strain softening and shear thinning are enhanced relative to those in the previous case of $\varepsilon = 0.3$, but the trends are entirely consistent. We note that the maximum in the τ_{yy} component of the stress is almost a half channel height away from the free surface. The flow is even more plug like, hence the almost equally spaced streamlines in the center of the channel. Observing the streamline patterns near the free surface, there is almost none of the streamline compression near the wall that was observed for the strain hardening rheology. These differences in extensional rheology can be summarized by examining the tangential velocity and its gradient along the free surface shown in Fig. 11. For the strain hardening rheology ($\varepsilon = 0.05$), the strain rate along the free surface is almost constant near the stagnation point ($\dot{\epsilon} \approx 0.3U/H$) then increases close to the contact point ($\theta = \pi/2$). For the strain softening rheologies, the effective shear and extensional viscosities in the neighborhood of the singularity are very low, so the material along the interface is not effectively accelerated. The result is a lower strain rate along the interface and a large peak near the point of contact. For $\varepsilon = 0.9$ the average strain rate near the stagnation point has dropped to $\dot{\epsilon} \approx 0.1U/H$.

B. Stability results

Once steady results are obtained, a linear stability analysis is performed for each case. By tracking the norm of the perturbation as a function of time, demonstrated in Fig. 12 for $\varepsilon = 0.90$, the stability of the flow can be determined. For this case, the initial perturbation introduced at time equals zero decays showing that the flow is stable (i.e., the real part of the eigenvalue is negative). The initial decay of the perturbation is very rapid

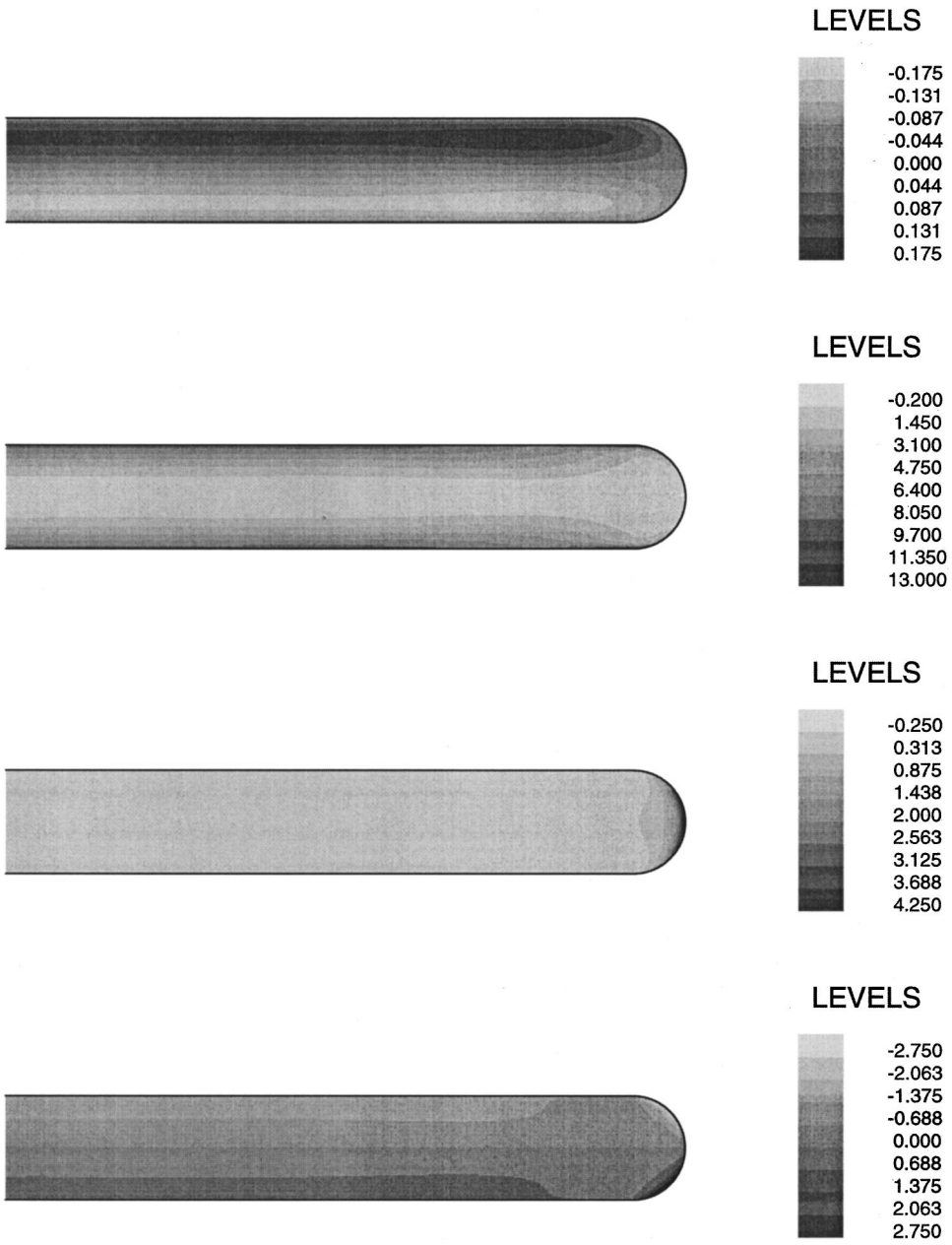

FIG. 8. Steady finite element results for strain hardening Phan-Thien–Tanner fluid with $\varepsilon = 0.05$, $Wi = 3.0$: from the top stream function, τ_{xx}, τ_{yy}, τ_{xy}.

because the disturbance excites many eigenmodes in the system. However at long times, the decay becomes single exponential indicating that only the eigenmode with the largest real eigenvalue remains and the growth/decay rate can be easily determined. From Fig. 12, we note that the real part of the eigenvalue increases monotonically with the Weissenberg number.

Figure 13 shows a similar set of results for the strain hardening rheology with

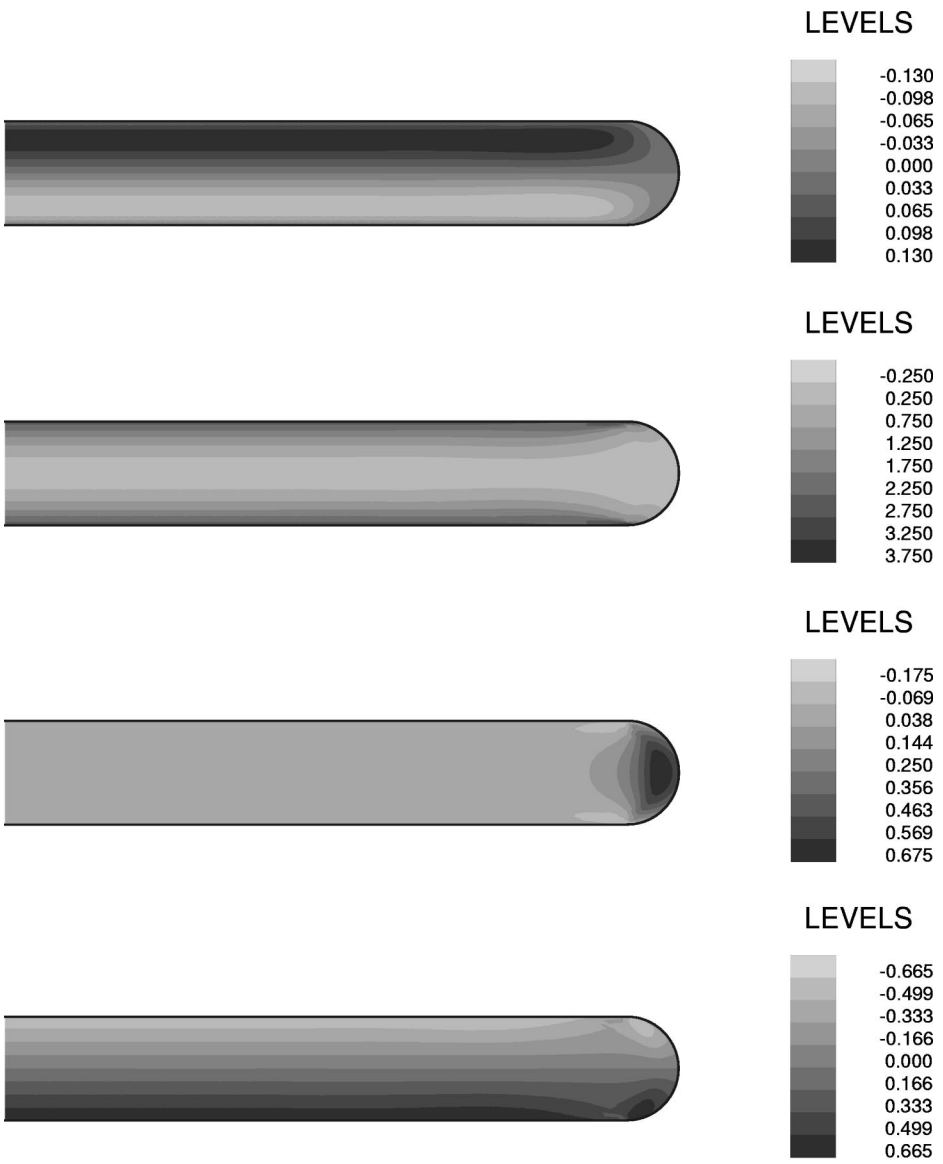

FIG. 9. Steady finite element results for strain softening Phan-Thien–Tanner fluid with $\varepsilon = 0.30$, $Wi = 3.0$: from the top stream function, τ_{xx}, τ_{yy}, τ_{xy}.

$\varepsilon = 0.05$. For low Weissenberg numbers we see very similar behavior to that in the previous case: the initial perturbation decays very rapidly initially before settling down to a single exponential decay. As the Weissenberg number increases, the perturbations decay more slowly and become oscillatory, and eventually the flow becomes unstable at $Wi \approx 4.8$. These results can be summarized by plotting the real part of the eigenvalue for the different values of ε as a function of the inverse Weissenberg number (cf. Fig. 15). For low Weissenberg numbers or strain softening rheologies, the eigenvalues remain negative (stable) and scale linearly with the inverse Weissenberg number. For the strain hardening materials at high enough Weissenberg numbers, the eigenvalues deviate from

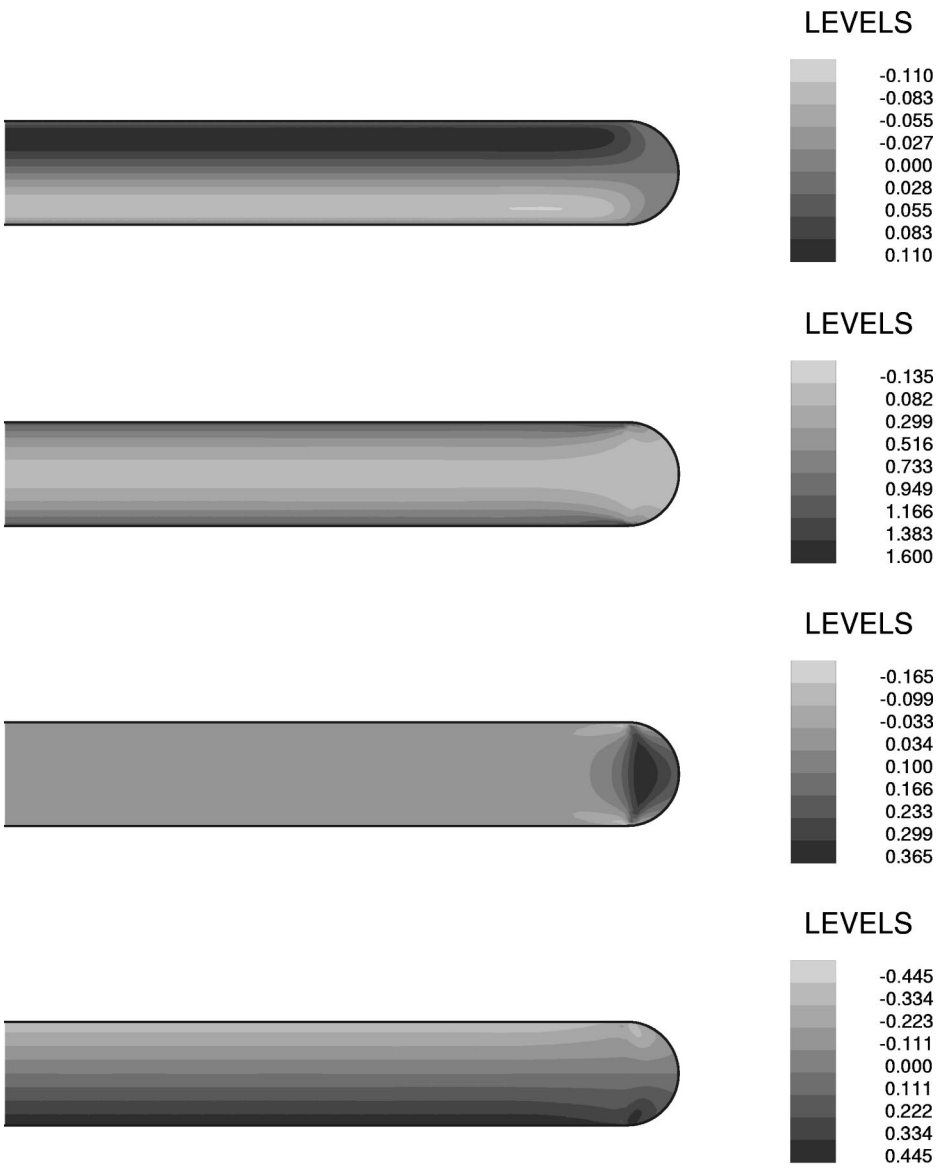

FIG. 10. Steady finite element results for strain softening Phan-Thien–Tanner fluid with $\varepsilon = 0.90$, $Wi = 3.0$: from the top stream function, τ_{xx}, τ_{yy}, τ_{xy}.

the linear trend, eventually becoming positive, indicating instability. Figure 14 shows that the stability behavior is not a function of the mesh resolution, length of the mesh, or the time step chosen for the transient calculation. For Weissenberg numbers higher than 3 only the longer meshes produced converged results for $\varepsilon = 0.05$.

Examining the eigenvectors obtained from the linear stability analysis, we find that the two regimes in the growth rate are characterized by very different spatial dependences of the eigenvectors. To compare we focus on $Wi = 5$ for strain softening and strain hardening rheologies. Figure 16(a) shows the steady velocity vectors for the strain softening rheology for $\varepsilon = 0.9$. The perturbation velocity vectors shown in Fig. 16(b) would be

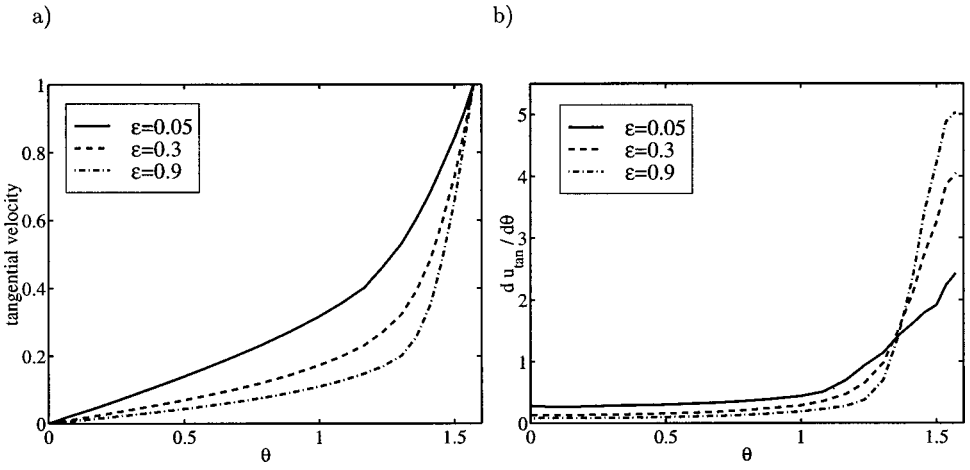

FIG. 11. Results along the free surface as a function of interface coordinate θ for various ε at $Wi = 3$: (a) tangential velocity $u_{\tan}$ and (b) gradient of velocity $\partial u_{\tan}/\partial\theta$. θ is defined as the angle along the semicircular interface from the stagnation point in the center of the channel.

superimposed on the steady solution. Because the flow is stable, the sizes of the perturbation vectors have been scaled so that the spatial dependence of the eigenvector can be observed. The perturbation far from the channel has completely died out leaving a swirling flow near the free surface. This eigenvector is consistent with the unstable flow pattern observed with the two color injection molding experiments (cf. Fig. 5) [Bulters and Schepens (2000a), 2000b].

The characteristic eigenvector for strain hardening rheologies at large Weissenberg numbers is shown in Fig. 17. Contrary to in the previous case, the perturbation velocities in the neighborhood of the interface have completely decayed. What remains is essentially an instability in the plane Poiseuille flow in the inlet channel. This can be confirmed by comparing finite element calculations in this injection molding flow with similar

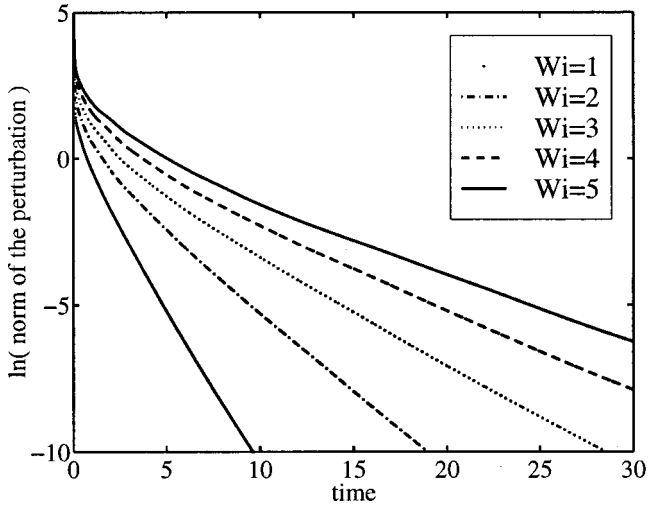

FIG. 12. Linear stability results for strain softening rheology with $\varepsilon = 0.90$ for various Weissenberg numbers.

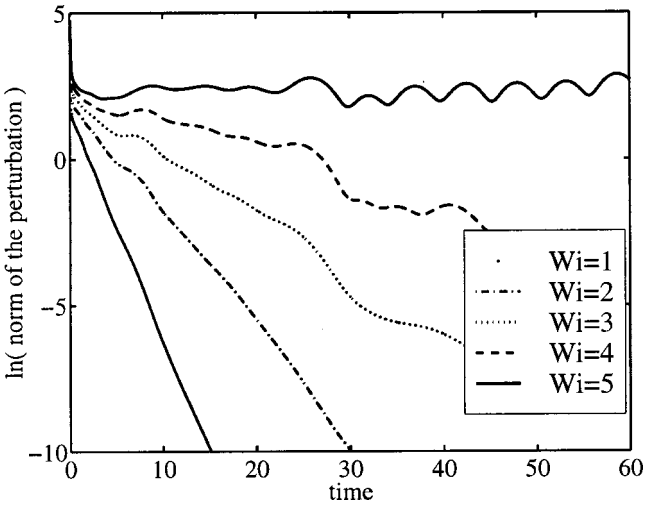

FIG. 13. Linear stability results for strain hardening rheology with $\varepsilon = 0.05$ for various Weissenberg numbers.

calculations in periodic planar Poiseuille flow shown in Fig. 18. The critical condition in the injection molding geometry ($Wi = 4.8$ for $\varepsilon = 0.05$) is slightly higher than that predicted for plane Poiseuille flow ($Wi = 4.3$). A more detailed analysis of these channel instabilities using both transient finite element and Chebyshev–Tau spectral methods was discussed by Grillet *et al.* (in press). While interesting for other reasons, the occurrence of channel instabilities is unfortunate in that they are not related to the flow mark surface defects which are the focus of this investigation. The important point is that the choice of constitutive equation affects not only the predictions of steady flow properties, but also the stability of the flow. For example, both the upper convected Maxwell model and the Oldroyd-B model are stable in plane Poiseuille flow [Gorodtsov and Leonov (1967); Wilson *et al.* (1999)].

IV. CONCLUSIONS

We have shown that the implicit DEVSS-G/SUPG transient finite element code presented by Grillet *et al.* (in press) can be used to investigate the stability of complex flows of polymer melts. This method was applied to a model injection molding flow where there was experimental evidence of a flow instability. Novel two color injection molding experiments were used to evaluate the potential mechanisms proposed for flow mark surface defects [Bulters and Schepens (2000a)]. Slip and upstream factors were ruled out by modifying the mold surface, gate, and screw designs, leaving the most likely explanation for the surface defects to be a flow instability during filling of the mold. Additional two color injection molding experiments in which the mold was only partially filled provided further evidence that the instability is localized in the fountain flow near the free surface.

With the goal of numerically predicting instabilities in injection molding flows, we applied a stabilized transient finite element method to a model injection molding flow. In order to test and develop the numerical method for this complex flow, simulations were performed using a one mode exponential Phan-Thien–Tanner model. The effect of extensional rheology on the steady flow and stability behavior was examined. In steady flows of strain hardening materials, large polymer stresses were found to build up along

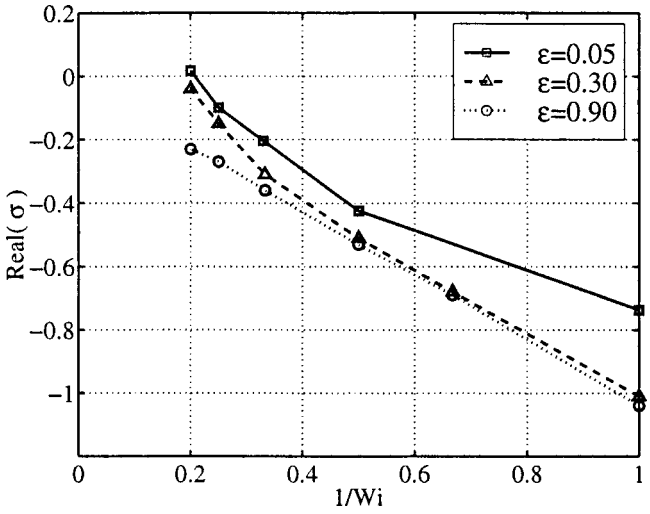

FIG. 14. Linear stability results for strain hardening rheology with $\varepsilon = 0.05$ with $Wi = 3$ for various time steps and meshes, given in Table I.

the free surface and extend downstream into the channel flow for some distance. Strain softening materials had much lower levels of polymer stress and the stress was localized away from the stagnation point on the free surface. Examination of the tangential velocity along the interface confirms that the more strain hardening material has a higher, more uniform strain rate in the neighborhood of the stagnation point.

Linear stability analyses were performed on the model injection molding flow. For strain hardening rheologies, a channel instability was predicted to occur far away from the free surface. The destabilization for Weissenberg numbers greater than 3 is in good agreement with predictions for planar Poiseuille flow [Grillet *et al.* (in press)]. For strain softening rheologies, the eigenvector for the most unstable eigenmode has almost com-

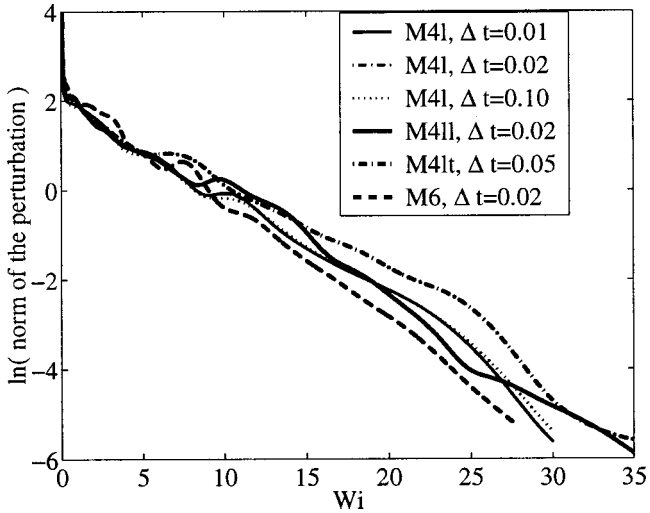

FIG. 15. Comparison of linear stability results for several extensional rheologies as a function of the inverse Weissenberg number.

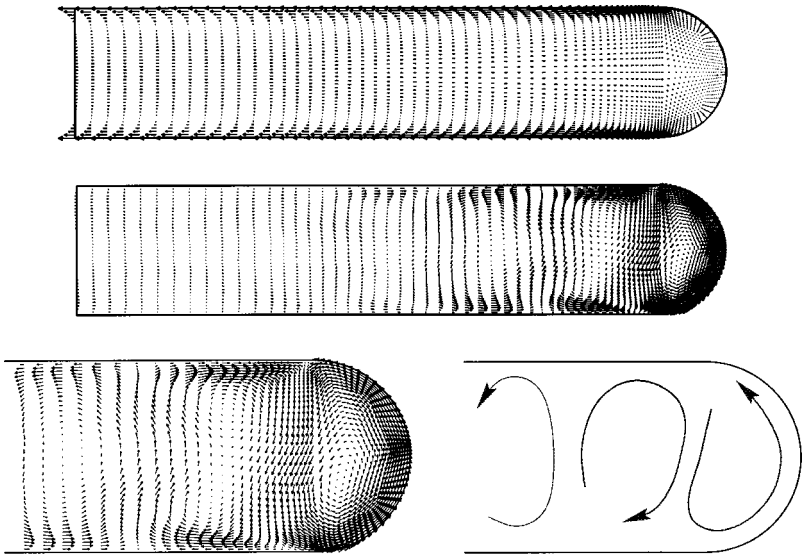

FIG. 16. Linear stability results for strain softening material with $\varepsilon = 0.90$ at $Wi = 5$: (a) steady velocity vectors; (b) most unstable eigenvector ($|u|*10^{+5}$); (c) closeup of swirling flow near the interface.

pletely decayed in the channel flow portion of the geometry and is instead concentrated as a swirling flow near the free surface. The velocity vectors of the most unstable eigenmode are in qualitative agreement with the experimentally observed instability [Bulters and Schepens (2000a)]. The growth rate for the swirling eigenmode increased monotonically with Weissenberg number but no instability was predicted for the range of Weissenberg numbers investigated in this study.

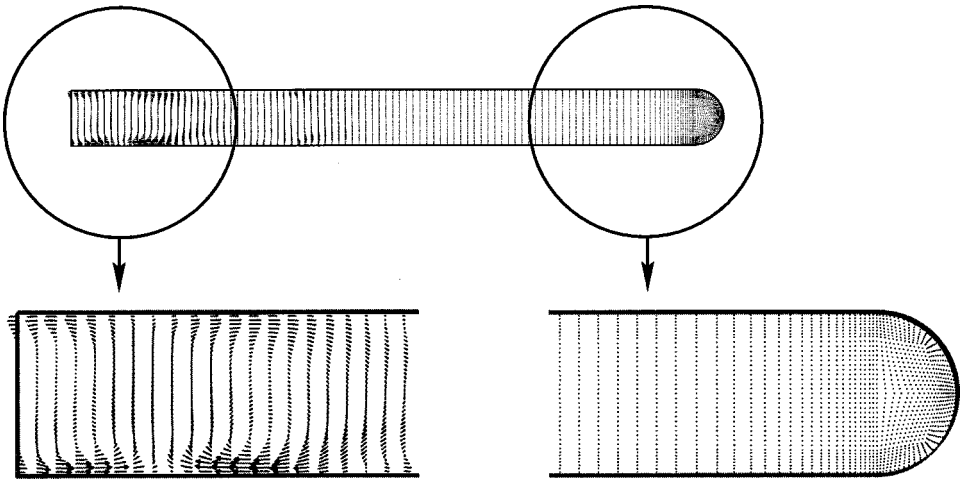

FIG. 17. Linear stability results for the most unstable eigenvector for strain hardening material with $\varepsilon = 0.05$ at $Wi = 5$.

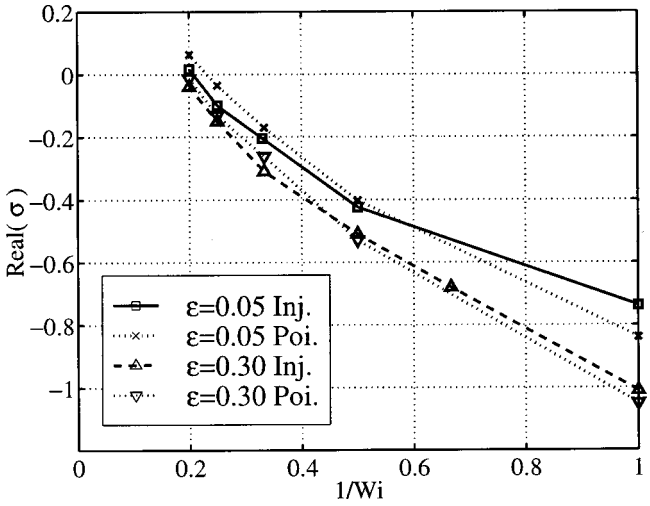

FIG. 18. Comparison of linear stability analysis for injection molding flow and Poiseuille flow [Grillet *et al.* (in press)].

ACKNOWLEDGMENT

This work was financially supported by the Dutch Polymer Institute.

References

Alves, M. A., F. T. Pinho, and P. J. Oliveira, ''Study of steady pipe and channel flows of a single-mode Phan-Thien–Tanner fluid,'' J. Non-Newtonian Fluid Mech. **101**, 55–76 (2001).

Baaijens, F. P. T., ''Mixed finite element methods for viscoelastic flow analysis: A review,'' J. Non-Newtonian Fluid Mech. **79**, 361–386 (1998).

Brooks, A. N. and T. J. R. Hughes, ''Streamline Upwind/Petrov Galerkin formulations for convection dominated flows with particular emphasis on the incompressible Navier–Stokes equations,'' Comput. Methods Appl. Mech. Eng. **32**, 199–259 (1982).

Brown, R. A., M. Szady, P. Northey, and R. C. Armstrong, ''On the numerical stability of mixed finite-element methods for viscoelastic flows governed by differential constitutive equations,'' Theor. Comput. Fluid Dyn. **5**, 77–106 (1993).

Bulters, M. and A. Schepens, ''The origin of the surface defect 'slip-stick' on injection moulded products,'' Paper IL 3-2, in *Proceedings of the 16th Annual Meeting of the Polymer Processing Society*, Shanghai, China, 2000a, pp. 144–145.

Bulters, M. and A. Schepens, ''Flow mark surface defects on injection moulded products: 1 Proposed mechanism,'' in *Proceedings of the Annual Meeting of the American Institute of Chemical Engineers*, Los Angeles, CA, 2000b.

Chang, M. C. O., ''On the study of surface defects in the injection molding of rubber-modified thermoplastics,'' ANTEC '94 (1994), pp. 360–367.

Denn, M. M., ''Extrusion instabilities and wall slip,'' Annu. Rev. Fluid Mech. **33**, 265–287 (2001).

Gorodtsov, V. A. and A. I. Leonov, ''On a linear instability of a plane parallel Couette flow of viscoelastic fluid,'' J. Appl. Math. Mech. **31**, 310–319 (1967).

Grillet, A. M., B. Yang, B. Khomami, and E. S. G. Shaqfeh, ''Modeling of viscoelastic lid driven cavity flow using finite element simulations,'' J. Non-Newtonian Fluid Mech. **88**, 99–131 (1999).

Grillet, A. M., A. C. B. Bogaerds, G. W. M. Peters, and F. P. T. Baaijens, ''Stability analysis of constitutive equations for polymer melts in viscometric flows,'' J. Non-Newtonian Fluid Mech. **103**, 221–250 (2002).

Guénette, R. and M. Fortin, ''A new mixed finite element method for computing viscoelastic flows,'' J. Non-Newtonian Fluid Mech. **60**, 27–52 (1995).

Hamada, H. and H. Tsunasawa, ''Correlation between flow mark and internal structure of thin PC/ABS blend injection moldings,'' J. Appl. Polym. Sci. **60**, 353–362 (1996).

Hinch, E. J., ''The flow of an Oldroyd fluid around a sharp corner,'' J. Non-Newtonian Fluid Mech. **50**, 161–171 (1993).

Hobbs, S. Y., ''The development of flow instabilities during the injection molding of multicomponent resins,'' Polym. Eng. Sci. **32**, 1489–1494 (1996).

Isayev, A. I., *Injection and Compression Molding Fundamentals* (Marcel Dekker, New York, 1987).

Kamal, M. R., E. Chu, P. G. Lafleur, and M. E. Ryan, ''Computer simulation of injection mold filling for viscoelastic melts with fountain flow,'' Polym. Eng. Sci. **26**, 190–196 (1986).

Kamal, M. R., S. K. Goyal, and E. Chu, ''Simulation of injection mold filling of viscoelastic polymer with fountain flow,'' AIChE J. **34**, 94–106 (1988).

King, R. C., M. R. Apelian, R. C. Armstrong, and R. A. Brown, ''Numerically stable finite element techniques for viscoelastic flow calculations in smooth and singular geometries,'' J. Non-Newtonian Fluid Mech. **29**, 147–216 (1988).

Larson, R. G., *Constitutive Equations for Polymer Melts and Solutions* (Butterworths, Boston, 1988).

Mavridis, H., A. N. Hrymak, and J. Vlachopoulos, ''Finite element simulation of fountain flow in injection molding,'' Polym. Eng. Sci. **26**, 449–454 (1986).

Mavridis, H., A. N. Hrymak, and J. Vlachopoulos, ''The effect of fountain flow on molecular orientation in injection molding,'' J. Rheol. **32**, 639–663 (1988).

Monasse, B., L. Mathieu, M. Vincent, J. M. Haudin, J. P. Gazonnet, V. Durand, J. M. Barthez, D. Roux and J. Y. Charmeau, ''Flow marks in injection molding of polypropylene: Influence of processing conditions and formation in fountain flow,'' in the *Proceedings of the 15th Annual Meeting of the Polymer Processing Society*, s'Hertogenbosch, The Netherlands (1999).

Reilly, F. J. and W. L. Price, ''Plastic flow in injection molds,'' SPE J. , 1097–1101 (1961).

Rose, W., ''Fluid-fluid interfaces in steady motion,'' Nature (London) **191**, 242–243 (1961).

Saramito, P., ''Efficient simulation of nonlinear viscoelastic fluid flows,'' J. Non-Newtonian Fluid Mech. **60**, 199–223 (1995).

Sato, T. and S. M. Richardson, ''Numerical simulation of the fountain flow problem for viscoelastic liquids,'' Polym. Eng. Sci. **35**, 805–812 (1995).

Shen, S.-F., ''Grapplings with the simulation of non-Newtonian flows in polymer processing,'' Int. J. Numer. Methods Eng. **34**, 701–723 (1992).

Tadmor, Z., ''Molecular orientation in injection molding,'' J. Appl. Polym. Sci. **18**, 1753–1772 (1974).

Talwar, K. K., H. K. Ganpule, and B. Khomami, ''A note on the selection of spaces in computation of viscoelastic flows using the *hp*-finite element method,'' J. Non-Newtonian Fluid Mech. **52**, 293–307 (1994).

Wilson, H. J., M. Renardy, and Y. Renardy, ''Structure of the spectrum in zero Reynolds number shear flow of the UCM and Oldroyd-B liquids,'' J. Non-Newtonian Fluid Mech. **80**, 251–268 (1999).

Wissbrun, K. F. (private communication, 2001).